dilute acid solution. The microradiographs show the evolution of the ions diffusing from the metal to the solution.

The small black zones on the left of each image in Fig. 2A, caused by corrosion pits on the metallic sheet, show the progressive erosion of the metal (negative absorption because of the subtraction). Light regions in the center of the images show the diffusion process, and dark zones correspond to hydrogen (H_2) bubbles, which reduce the layer thickness of the Zn^{2+} ions and locally decrease the x-ray absorption. We do not see, as was naïvely expected, a front of Zn^{2+} ions moving perpendicular to the zinc electrode because, in fact, this chemical reaction is associated with complicated microscopic phenomena, such as the creation of a turbulent medium caused by the gas release. Therefore, this experiment demonstrates that this phenomenon is a complex process that cannot be studied with a one-dimensional Fick's law.

In the reaction with the zinc pellets (Fig. 3), we see the evolution of a front of Zn^{2+} ions, limited by the walls of the cell, complicated by the production and movement of H_2 bubbles and by the concentration gradient [decreases from the top left of each image (where the zinc pellets were situated) to the bottom right]. These images show what happens in a general case, without any particular geometry for the metallic specimen. The spherical edges of the front give rise to two menisci (observed from t = 360 s). These menisci result from the formation of H_2 bubbles. All of these images show the influence of the gas release in the creation of a turbulent medium that leads to heterogeneous diffusion.

To quantify the distribution of the Zn^{2+} ions moving into the liquid, we obtain μt maps for each stage of the diffusion and convert them into concentration maps. It is possible to see how a given concentration profile $C(x,y_0,t)$ (Fig. 4A) or a local concentration $C(x_0,y_0,t)$ at a given point (x_0,y_0) (Fig. 4B), expressed in zinc atoms per H_2O molecule, changes with time. We can also delimit isoconcentration lines on each initial microradiograph (Fig. 4C).

Our technique, characterized by its ease of operation (a modified scanning electron microscope), good sensitivity, and sufficient spatial resolution for this type of study, offers the possibility of evaluating the local concentration of the solvated species, even in a colorless solution, such as zinc in hydrochloric acid. We believe that this technique can be adapted to a wide field of applications, including the visualization of ionic species migration during electrochemical processes, the diffusion of ionic particles in a porous medium, or the diffusion of K^+, Na^+, and Ca^{2+} ions in biological materials with a lateral resolution of a few micrometers.

REFERENCES

1. J. Philibert, *Atom Movement: Diffusion and Mass Transport in Solids* (Les Editions de Physique, Les Ulis, France, 1991).
2. A. Moelwyn Hughes, *The Chemical Statics and Kinetics of Solutions* (Academic Press, London, 1971), chap. 5.
3. S. Rondot, J. Cazaux, D. Erre, D. Mouze, P. Trebbia, paper presented at the Fourth International Conference on X-ray Microscopy, Chernogolovka, Russia, 20 to 24 September 1993.
4. J. Benard, A. Michel, J. Philibert, J. Talbot, *Métallurgie Générale* (Masson, Paris, ed. 2, 1991), pp. 416–417.
5. S. Rothman, K. K. Gonez, B. W. Loo Jr, in *X-ray Microscopy III*, A. G. Michette, G. R. Morrison, C. J. Buckley, Eds. (Springer-Verlag, Berlin, 1992), pp. 373–383.
6. P. Anderson, S. E. P. Dowker, J. C. Elliott, G. H. Dibdin, *ibid.*, pp. 435–437.
7. X. Thomas, J. Cazaux, D. Erre, D. Mouze, P. Collard, *ibid.*, pp. 190–194.
8. J. Cazaux *et al.*, paper presented at Euromat '93, 3rd European Conference on Advanced Materials and Processes, Paris, June 1993.
9. D. Erre, thesis, University of Reims (1993).
10. J. Cazaux, *Microsc. Microanal. Microstruct.* **4**, 513 (1993).
11. H. Ade *et al.*, *Science* **258**, 972 (1992).
12. D. Erre, D. Mouze, X. Thomas, J. Cazaux, in *Progress in Digital X-ray Projection Microscopy*, P. B. Kenway *et al.*, Eds. (Institute of Physics Conference Ser. 130, IOP Publ., London, 1993), p. 567.
13. N. Watanabe *et al.*, *Jpn. J. Appl. Phys.* **31**, L1571 (1992).
14. J. Pine and J. R. Gilbert, in (*5*), pp. 384–387.
15. J. O'M. Bockris and A. K. N. Reddy, *Modern Electrochemistry* (Plenum, New York, 1970), vol. 1.
16. M. Pourbaix, *Atlas d'Equilibres Électrochimiques à 25°C* (Gauthier-Villars, Paris, 1963).

4 November 1993; accepted 7 February 1994

From Static to Kinetic Friction in Confined Liquid Films

Günter Reiter, A. Levent Demirel, Steve Granick*

The transition from rest to sliding contact of atomically smooth solids separated by molecularly thin liquid films was studied. The films could be deformed nearly reversibly to a large fraction of the film thickness. The modulus of elasticity and yield stress were low, considerably less than for a molecular crystal or glass in the bulk. The transition to dissipative sliding was typically (but not always) discontinuous. The dissipative stress was then nearly velocity-independent. The similar response of monolayers strongly attached to the solid surfaces, presenting a well-defined interface for sliding, suggests that the physical mechanism of sliding may involve wall slip.

Not enough is understood about friction (*1–5*). This impedes progress not only on workaday problems of tribology but also on other complex dynamical problems such as earthquakes. An essential fact to appreciate is that solid bodies in contact are nearly always lubricated, either by liquids or additives that are intentionally added or by condensed vapors. However, confined liquids were recently found to exhibit patterns of friction normally associated with the deformation of solids. This result, first proposed in the engineering literature (*6–8*), has now also emerged for films that are molecularly thin (*9, 10*). However, in all of these experiments the displacements were large, too large to investigate decisively the transition from static to kinetic friction.

A surface forces apparatus with oscillatory shear attachment was used (*10, 11*). In previous work we investigated the perturbed liquid-like response of thicker confined liquid films (*5, 10*); here we investigate the solidity (*4, 5, 9, 10*) of thinner films. The liquid of interest was confined between two circular parallel sheets of atomically smooth mica whose diameter was vast (≈10 μm) compared to the molecularly thin distance between them. The film thickness and area of flattened contact were measured by multiple-beam interferometry. Sinusoidal shear forces were applied by a piezoelectric element. A second sensor piezoelectric element was used to detect the resulting response, which was compared with the force required to deform this element when no liquid was present (*12*). The temperature was 27°C.

The contributions of the mechanical response of the apparatus, especially of the glue that attached the mica to the rest of the device (*11*), were calibrated with the mica surfaces in dry adhesive contact. Measurements with confined liquids were then analyzed with the use of a model in which the calibrated apparatus response coupled mechanically with the thin-film sample (*12*). With regard to the uncertainties of calibration, a conservatively low bound of glue stiffness was assumed. Consequently, deformations of the thin-film samples might be larger (perhaps by up to 50%) than those we describe below, but not smaller.

Materials Research Laboratory and Department of Materials Science and Engineering, University of Illinois, Urbana, IL 61801, USA.

*To whom correspondence should be addressed.

The linear viscoelastic response is illustrated in Fig. 1; the significance of linear response is that the ultra-small deformations did not perturb the film structure. The data refer to a film of squalane (SQA), $C_{30}H_{62}$, 2 nm thick. Squalane is a small branched hydrocarbon often used as a model lubricant. The deflection amplitude, d_o, rises linearly with driving force amplitude in Fig. 1A. Force was applied in a periodic fashion, $f(t) = f_o \sin \omega_1 t$, where t is time, ω_1 is the radian frequency, and f_o is the force amplitude. The resulting deflection was periodic at the same frequency, with amplitude d_o, but retarded in phase. At a yield point, indicated by the arrow in Fig. 1A, deflection jumped discontinuously. We identify this peak elastic force with the static friction.

A low level of elastic energy per molecule was stored at this yield point. Elastic energy is, of course, simply calculated as the product of the driving force and the resulting deformation. For the data in Fig. 1, this value is only $\approx 0.1\ kT$ per molecule (k is the Boltzmann constant and T is the absolute temperature).

These data are also conveniently quantified as viscoelastic moduli. Force was normalized by area to give stress. By conventional methods (*13*), the elastic and dissipative responding stresses were calculated from the components of deflection that were in phase and out of phase with the driving stress. These stress values were normalized by strain to give the elastic and dissipative shear moduli, G′ and G″, respectively, of Fig. 1B. The values for G′ exceeded those for G″, reflecting predominant elasticity. Control experiments indicated no frequency dependence over the frequencies studied, 0.03 to 20 Hz, confirming that the films acted as classic viscoelastic solids.

This level of elasticity is three orders of magnitude less than would be typical of a glass or crystal in the bulk (*13*). It is difficult to reconcile this low elasticity with the crystalline or glassy states that researchers in this laboratory and in others (*4, 5, 14–17*) have supposed to cause solidity of ultrathin films. In addition, G′ and G″ were constant up to deflections amounting to a large fraction of the film thickness, again in contrast to a crystal or glass in the bulk. Control experiments in other systems confirmed this phenomenon. This thin liquid film behaved as a "soft" solid.

The experimental observation is clear, although explanation, in terms of collective caged motions, is still conjectural (*18*). In fact, this "soft" solidity served a useful function: It ensured that yield took place somewhere in the thin film rather than by the degradation of the sliding surfaces.

Although deformation below the yield transition was absolutely sinusoidal, it was not so after the yield. The distortions of waveforms were measured when the deformation caused the film to yield (Fig. 2). We interpret the breaks in the waveforms to indicate that "stick" (at small deflections) gave way to "slip" (at larger deflections). Such transitions were quantitatively reproducible during many repetitions. The distortions in Fig. 2 happen at the same fraction of a period independent of frequency, indicating a constant yield stress at the point of slip. Fourier transforms of such distorted waveforms can be analyzed in the context of patterns of stick-slip behavior that have been much discussed recently (*19*).

Here we analyze the simplest case, the motion at the frequency of the drive force, ω_1. This analysis was done not just for simplicity but also because, owing to the cancellation of higher harmonic contributions, only the fundamental frequency response of a sinusoidally periodic experiment determines the energy that is lost during a cycle of oscillation (*20*).

As in earlier work (*5*), we found that the reducing variable necessary to analyze the dissipative stress at the fundamental frequency at large deformation was velocity. This conclusion followed because, when amplitude and frequency were varied separately, the dissipative stress depended only on their product. Here we have defined peak velocity as the product of frequency and deflection amplitude.

The dissipative stress after yield is associated with the kinetic friction. The velocity dependence is shown in Fig. 3. Here, with squalane films in a different experiment, the elastic and dissipative stress ($\sigma_{o,el}$ and $\sigma_{o,diss}$, respectively) are plotted against peak velocity on log-log scales. Dissipative stress was rate-independent in the range of 1 to 100 nm sec^{-1}, with a strong upturn at larger velocities. This near rate independence of $\sigma_{o,diss}$ decisively confirms measurements of Israelachvili and McGuiggan, in which the rate was varied over a smaller range in steady-state sliding (*9*). There was a persistent elastic stress even after yield, indicating a deformed structure that could not fully relax during the period of an oscillation. However, $\sigma_{o,el}$ decreased as the deflection increased (at constant frequency), indicating that faster movement resulted in lower elasticity. The weak dependence of dissipative stress on velocity (Fig. 3) is unlike any response of a bulk liquid. This weak dependence suggests that the mechanism of flow after yield may not involve a solid-to-liquid transition, as has been widely assumed; an alternative interpretation is presented below.

We now contrast the transition from

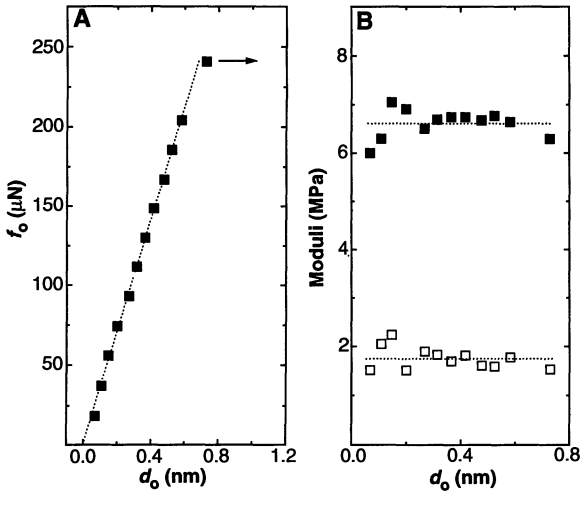

Fig. 1. Viscoelastic measurements of squalane films confined between atomically smooth sheets of mica at a thickness of 2.0 nm and a net normal pressure of ≈1 MPa. Data are taken at 1.3 Hz in the direction of increasing deflection amplitude (d_o). (**A**) Force amplitude (f_o) versus d_o. The arrow indicates the yield point. (**B**) For the same data shown in (A), storage modulus, *G′* (filled squares), and loss modulus, *G″* (open squares), plotted against deflection amplitude.

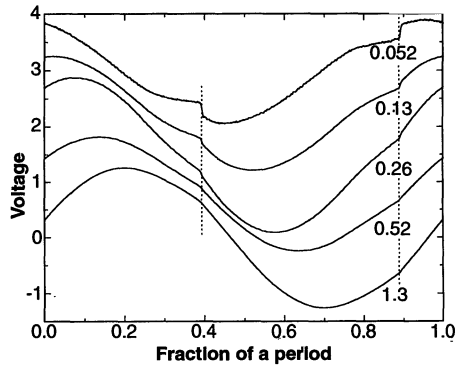

Fig. 2. Distortions observed in the responding waveforms when the deflection was so large as to pass the yield point during a cycle of oscillation. Amplitude is constant and frequency is varied, so peak velocity during oscillation is varied. Voltage (arbitrary units) is plotted against the fraction of a period. Note that the yield, indicated by vertical dashed lines, happens at the same fraction of a period regardless of frequency, indicating a constant yield stress at the point of slip (frequency values by each trace are in hertz). In contrast, motion below the yield transition was sinusoidal.

static to kinetic response in three systems: a thin film of SQA liquid, a dry monolayer of octadecyl chains (OTE) strongly bound to the mica surfaces, and a thin film of perfluoroether liquid. Perfluoroethers, of which perfluoroheptaglyme [$CF_3O(CF_2CF_2O)_7\,CF_3$; PFG] is an example, are an important family of lubricants. The elastic and dissipative stresses are plotted against peak deflection in Fig. 4. Because the frequency was constant, deflection after the yield point was proportional to velocity.

First we compare the friction associated with the confined liquid, SQA, to that in a system (OTE) in which only solid friction should be possible, because the strongly bound monolayers present a well-defined interface for sliding. The procedure to blanket the native mica surface with a self-assembled monolayer of condensed octadecyl chains has been described (*21*). The procedure was modified to lower the adhesion between two opposed layers, to the point where tangential slip could be studied. The pattern of yield stress, followed by a kinetic state of predominant dissipation, was essentially the same for OTE as for SQA.

In fact, these data for SQA and OTE are reminiscent of usual stress-strain relations of many bulk solids: metals, polymers, granular powders (*22, 23*), and concentrated colloidal suspensions (*24–26*). We suggest tentatively that in the present systems, as for the yield of bulk solids, the mechanism of rate-independent friction may also involve wall slip. Motion would then be accomplished by the sliding of layers past one another rather than by a more homogeneous liquid-like deformation (*13, 27*). Certainly in the OTE system, the only plausible mechanism of sliding is that the opposed monolayers, each one strongly bound to a mica surface, slid over one another.

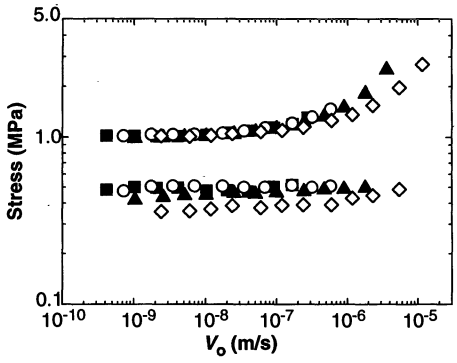

Fig. 3. Velocity dependence of stress for squalane confined between atomically smooth sheets of mica at a thickness of 2.3 nm and a net normal pressure of ≈1 MPa. Dissipative stress (top curve) and elastic stress (bottom curve) are plotted on log-log scales against peak velocity during a cycle of oscillation, as described in the text. The oscillation drive amplitudes were 15 nm (squares), 20 nm (circles), 25 nm (triangles), and 50 nm (diamonds). The frequency was varied from 0.05 to 260 Hz.

In other experiments with SQA confined between OTE monolayers, which are only partially wet by organic liquids because the surface energy of OTE is so low (*21*), we also observed rate-independent sliding. The position of the slip plane should be a function of the surface energy. In the present experiments with mica, slip may occur within the thin film; adsorbed SQA layers may slip against one another. For solids of low surface energy, such as OTE, slip may take place at the solid wall.

What might be the underlying structural changes? In the yield of bulk solids, an increase of volume appears to be the mechanism by which rate-independent sliding is achieved at constant pressure (*22*). Similarly, increases in film thickness (though by less than the experimental resolution of 1 to 2 Å) are reasonable to expect in the present systems and are predicted in computer simulations of confined liquids (*16*). Such increases should be accompanied by forces that act in the direction normal to the sliding direction. These normal forces, which are not predicted by standard lubrication theories (*1*), would then help to prevent the solid bodies from making actual contact during sliding. This would imply lower adhesion during sliding than in the stationary state. We have observed this effect.

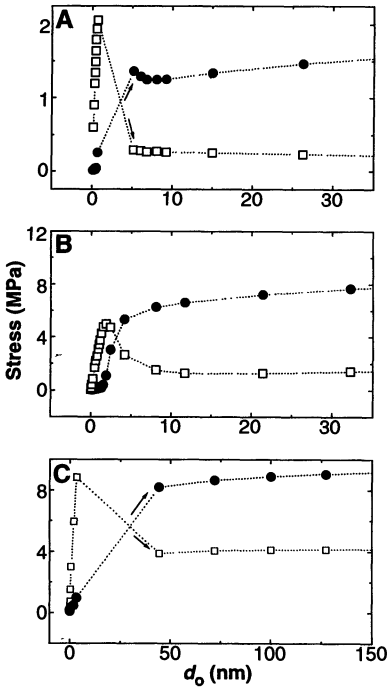

Fig. 4. Transition from static to kinetic friction in three systems. Data are taken at 1.3 Hz in the direction of increasing deflection amplitude, d_o. Dissipative stress (open squares) and elastic stress (filled circles) are plotted versus d_o. Note that d_o is proportional to peak velocity. (**A**) Squalane system specified in Fig. 1. (**B**) Perfluoroheptaglyme confined between atomically smooth mica sheets at a thickness of 1.2 nm and net normal pressure of ≈1 MPa. (**C**) Octadecyl chains strongly attached to the solid surfaces to form opposed monolayers with a total thickness of 5 nm. The OTE monolayers are in dry adhesive contact (net normal pressure of ≈0 MPa).

The hysteresis and reversibility of such experiments are also worth comment. As the deflection amplitude during oscillation was lowered, at some point of low deflection the system would spring from the kinetic sliding back into the elastic solid state. The point of these reverse transitions was not, however, reproducible. The transition point appeared to depend either on fluctuations within the system or on small disturbances such as vibrations in the room; we conjecture that this dependence reflected irregular nucleation events. Apart from these points close to the transition that suggest a metastable response, the behavior in SQA and OTE systems could be recycled forward and backward for hours during repeated oscillations, indicating the absence of surface degradation.

In other systems, we found that the dissipative stress after yield was higher than the yield stress—the kinetic friction exceeded the static friction. This relation is illustrated by the behavior of PFG (Fig. 4B). In linear responses at small deformations, the viscoelastic moduli ($G' = 4.2$ MPa and $G'' = 0.2$ MPa for the data in Fig. 4B) were comparable to those of squalane shown in Fig. 1. The large dissipative stress after yield is consistent with previous reports that the friction of perfluorinated monolayers is unusually large (*28*). In addition, there was no zone of rate-independent response. In this sense, the response was reminiscent of the perturbed liquid-like behavior studied previously (*5*). Patterns of this kind were also observed for SQA and the other liquids referred to above, but only at lower normal pressures. Although we do not offer an explanation of this difference, we do note that the tendency toward more snappy yield with increased normal pressure is intuitively reasonable. The contrast between the continuous transition of PFG and the discontinuous transitions of OTE and SQA illustrates the danger of generalizing about the transition between static and kinetic friction.

This study shows that molecularly thin liquid films in the elastic rest state are very different from solids in the bulk: They are much weaker, and more deformable, than a molecular crystal or glass. The transition to the kinetic state is reminiscent of the "shear melting" of colloids; however this phenomenon may reflect wall slip, not a solid-liquid transition. "Soft" elasticity in the rest state helps one to understand a useful function of

lubrication: At the start-up of motion, yield occurs within the thin liquid film rather than by the degradation of solid surfaces.

REFERENCES AND NOTES

1. I. L. Singer and H. M. Pollock, Eds., *Fundamentals of Friction* (Kluwer Academic, Dordrecht, Netherlands, 1992).
2. J. N. Glosli and G. M. McClelland, *Phys. Rev. Lett.* **70**, 1960 (1993).
3. B. N. J. Persson, *ibid.* **71**, 1212 (1993).
4. H. Yoshizawa, P. McGuiggan, J. Israelachvilli, *Science* **259**, 1305 (1993); M. L. Gee, P. M. McGuiggan, J. N. Israelachvili, *J. Chem. Phys.* **93**, 1895 (1990).
5. S. Granick, *Science* **253**, 1374 (1991).
6. F. W. Smith, *Wear* **2**, 250 (1959).
7. S. Bair and W. O. Winer, *J. Tribology* **114**, 1 (1992), and references therein.
8. C. R. Evans and K. L. Johnson, *Proc. R. Soc. London Ser. A* **356**, 215 (1977), and references therein.
9. J. N. Israelachvili and P. M. McGuiggan, *Science* **241**, 795 (1988).
10. J. Van Alsten and S. Granick, *Phys. Rev. Lett.* **61**, 2570 (1988).
11. J. Peachey, J. Van Alsten, S. Granick, *Rev. Sci. Instrum.* **62**, 463 (1991).
12. H.-W. Hu, thesis, University of Illinois at Urbana–Champaign (1992).
13. J. D. Ferry, *Viscoelastic Properties of Polymers* (Wiley, New York, ed. 3, 1980).
14. M. Schoen, C. L. Rhykerd, D. J. Diestler, J. H. Cushman, *Science* **245**, 1223 (1989).
15. P. A. Thompson and M. O. Robbins, *ibid.* **250**, 792 (1990).
16. P. A. Thompson, G. S. Grest, M. O. Robbins, *Phys. Rev. Lett.* **68**, 3448 (1992).
17. H. Yoshizawa and J. Israelachvili, *J. Phys. Chem.* **97**, 11300 (1993).
18. H.-W. Hu and S. Granick, *Science* **258**, 1339 (1992).
19. M. de Sousa Vieira, G. L. Vasconcelos, S. R. Nagel, *Phys. Rev. E* **47**, R2221 (1993), and references therein.
20. S. Onogi, T. Masuda, T. Matsumoto, *Trans. Soc. Rheol.* **14**, 275 (1970).
21. C. R. Kessel and S. Granick, *Langmuir* **7**, 532 (1991).
22. H. M. Jaeger and S. R. Nagel, *Science* **255**, 1523 (1992).
23. M. J. Adams, in (*1*), pp. 183–207.
24. B. J. Ackerson and N. A. Clark, *Phys. Rev. Lett.* **46**, 123 (1981).
25. L. B. Chen *et al.*, *ibid.* **69**, 688 (1992), and references therein.
26. M. J. Stevens, M. O. Robbins, J. F. Belak, *ibid.* **66**, 3004 (1991).
27. Discontinuities of this kind were also observed for linear alkanes (undecane and dodecane), methylundecane, and the globular-shaped molecule octamethyl-cyclotetrasiloxane (OMCTS). The significance of the control experiment with OMCTS was to show that a conceivable coil stretch of the chain-like molecules could not explain the yield transition in general.
28. R. M. Overney *et al.*, *Nature* **359**, 133 (1992), and references therein.

29. We dedicate this paper to David Tabor on the occasion of his 80th birthday. We thank B. Cabane, J. D. Ferry, J. N. Israelachvili, K. Johnson, and J. Klein for discussions; C. R. Kessel, J. Peanasky, and L. Cai for assistance with measurements involving OTE monolayers; and W. R. Jones of the National Aeronautics and Space Administration–Lewis Space Center for donating the PFG. Supported by the Exxon Corporation and by the taxpayers of the United States through grants from the National Science Foundation (Tribology Program, NSF-MSM-92-02143) and the Air Force Office of Scientific Research (AFOSR-URI-F49620-93-1-02-41).

23 September 1993; accepted 31 January 1994

Defects in Carbon Nanostructures

O. Zhou, R. M. Fleming, D. W. Murphy, C. H. Chen, R. C. Haddon, A. P. Ramirez, S. H. Glarum

Previous high-resolution electron microscopy (HREM) observations of the carbon nanotubes have led to a "Russian doll" structural model that is based on hollow concentric cylinders capped at both ends. The structures of the carbon nanotubes and particles were characterized here by bulk physical and chemical property measurements. The individual nanostructure is as compressible as graphite in the *c* axis, and such nanostructures can be intercalated with potassium and rubidium, leading to a saturation composition of "MC_8." These results are counter to expectations that are based on a Russian doll structure. HREM after intercalation with potassium and deintercalation indicates that individual nanoparticles are a "paper-mache" of smaller graphite layers. Direct current magnetization and electron spin resonance measurements indicate that the electronic properties of the nanostructures are distinctly different from those of graphite. Although the nanostructures have distinct morphologies and electronic properties, they are highly defective and have a local structure similar to turbostratic graphite.

Modification of the spark erosion technique (*1*, *2*) for the synthesis of fullerenes has led to the discovery (*3*) and preparation of macroscopic quantities of carbon nanotubes (*4*). HREM images have been used to construct a model based on hollow concentric cylinders capped at both ends by curved sections (*3*, *4*). Concentric, almost spherical nanoparticles (onions) with hollow centers are also formed along with the tubes during spark erosion. Similar spherical nanoparticles are formed upon the *e*-beam irradiation of carbon soot particles and graphite (*5*). Popular models of these nanostructures could be described as nested Russian doll structures with concentric shells of large fullerene-like molecules.

Despite the appeal of the Russian doll model, defects of various forms have been apparent in published HREM images of carbon nanostructures (mixtures of tubes and onions). Amorphous carbon deposits have been noted on both the outer surface and in the center of the nanotubes (*3*, *4*). Discontinued graphite sheets can be found in both the nanotubes (*4*) and onions (*5*) by tracing of the lattice fringes. Dislocations have been discussed by Harris and colleagues (*6*). In one case, the transmission electron microscope (TEM) image of an uncapped tube viewed end-on resembles a spiral more than concentric cylinders (*7*). Even when defects are present, our computer simulations (Fig. 1) show that edge dislocations parallel to the tube axis are difficult to observe when they are projected normal to the tube axes (because of the morphology, most of the nanotubes can only be viewed along this direction). Thus, the observation of the same number of HREM lattice fringes on either side of the hollow center does not guarantee a perfect, nested fullerene structure.

Because of the limitations of HREM, we have sought to address the structural question through bulk physical and chemical properties. The premise of our approach is that the distance between adjacent shells in nested structures would be relatively unaffected by pressure (in contrast to the high interlayer compressibility in graphite), and that the intershell "galleries" within a nested nanostructure would be inaccessible to intercalation (just as is the interior of a C_{60} molecule).

The material used in this study was synthesized by the method of Ebbesen and Ajayan (*4*) and included samples prepared at AT&T and Rice University. The samples contained mostly tubes and onions, as shown by the representative HREM pictures in Fig. 2. The ratio of tubes to onions varied among experiments. The smallest nanotubes had two concentric graphitic shells. Most contained 20 to 30 layers with an intershell distance of ~3.4 Å, inner diameters of ~20 to 30 Å, and lengths greater than 1 μm. The ends always appeared to be closed in HREM images.

A powder x-ray diffraction pattern of a typical sample is shown in Fig. 3A. The pattern can be indexed on the basis of the hexagonal close-packed "graphite" unit cell with the *c* axis enlarged from 6.71 to 6.88 Å while the same C–C bond length is kept. This pattern is consistent with the findings of an earlier report (*8*) and is remarkably similar to the pattern of turbostratic graphite (*9*, *10*). The symmetrical (002) peak probes the average intershell spacing within each nanoparticle and is broadened from the finite number of layers in a single particle. The average interlayer spacing of 3.44 Å is 0.09 Å larger than that of crystalline graphite and reflects the lack of positional correlation between carbon atoms in different

AT&T Bell Laboratories, Murray Hill, NJ 07974, USA.